Journal of Materials Chemistry A

Accepted Manuscript

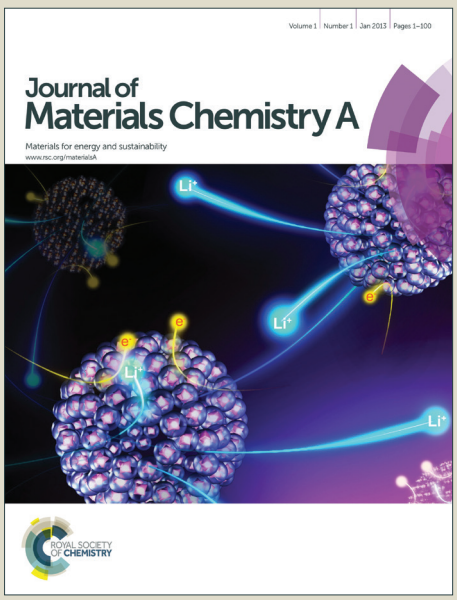

ROYAL SOCIETY OF CHEMISTRY

www.rsc.org/materialsA

Journal of Materials Chemistry A
Journal of Materials Chemistry A

Full Paper

Polyhedral $LiNi_{0.5}Mn_{1.5}O_4$ with excellent electrochemical properties for lithium-ion batteries

Zhanjun Chen,[a] Ruirui Zhao,[a] Peng Du,[a] Hang Hu,[a] Tao Wang,[a] Licai Zhu,[a]

Hongyu Chen*[a,b,c]

Alternative micro-sized $LiNi_{0.5}Mn_{1.5}O_4$ spinel with octahedral structure (showing only one type of {111} crystal face) or chamfered polyhedral structure with extra other faces have been synthesized *via* a controllable method. A possible growth model, Complexing-Pyrolyzing-Oriented, is also proposed for the formation of chamfered polyhedral $LiNi_{0.5}Mn_{1.5}O_4$ spinel based on the experimental results in this paper. The chamfered polyhedral $LiNi_{0.5}Mn_{1.5}O_4$ can provide a large capacity of 103 mAh g^{-1} even at a discharge rate as high as 50 C, which is far superior to that of the octahedral one. Besides, the capacity retentions of the chamfered polyhedral composites are found to be 90.82 % at 25 °C after 500 cycles and 90.00 % at 55 °C after 200 cycles, respectively, which are also better than those of octahedral one. These results represent the first experimental evidence for lattice-plane anisotropy in $LiNi_{0.5}Mn_{1.5}O_4$ crystal. Moreover, the pseudo-sphere structure is benefit to obtaining high volumetric energy density and excellent processability in practical application. In a word, we have firstly revealed that, through chamfering octahedron to pseudo sphere-liked polyhedron rather than doping or coating, a micro-sized $LiNi_{0.5}Mn_{1.5}O_4$ spinel with good compatibility between energy/power density and cycle life without other properties sacrifice can be synthesized successfully.

1. Introduction

Lithium-ion batteries (LIBs) have been widely applied in hybrid electrical vehicles (HEV), electrical vehicles

(EV), electric motor cycles and the smart grid system.[1-3] However, new cathodes with high energy/power density, long lifetime and low cost are necessary to be developed for the wider application of the LIBs in the potential mass market of electrical vehicles, which are urgent to be exploited to alleviate the continually increased CO_2 emissions and noise pollution.[4-6] More recent, spinel $LiNi_{0.5}Mn_{1.5}O_4$ was considered as one of the most promising cathode materials due to the following reasons: i) a high voltage plateau at around 4.75V, making its energy density 20% and 30% higher than that of conventional $LiCoO_2$ and $LiFePO_4$ materials, respectively;[7,8] ii) three-dimensional framework structures are helpful for avoiding the co-insertion of bulky species such as solvent molecules, leading to a stable cycle performance under room temperature; iii) the main raw materials (Ni and Mn) of $LiNi_{0.5}Mn_{1.5}O_4$ are abundant in the earth and also low costly. Unfortunately, the $LiM_{0.5}Mn_{1.5}O_4$ (M=Mn, Ni, Co, Cu, Fe or Cr) spinel compounds easily suffer from the Mn ions dissolution from (111) surface due to lattice modifications accompanied by the Jahn-Teller effect during cycling, especially at elevated temperatures, causing significant capacity loss during cycling.[6,9-14] Besides, compared with spinel $LiMn_2O_4$, the rate performance of spinel $LiNi_{0.5}Mn_{1.5}O_4$ is poorer due to lower diffusion coefficient [15-17] or lattice parameters[18-20].

To improve the electrochemical properties of spinel $LiNi_{0.5}Mn_{1.5}O_4$, a lot of approaches have been adopted. Surface coating is the most widely used approach for effectively improving the cycle performance due to the direct interaction between the electrolyte and the active materials can be avoid, but it reduces the capacity per unit mass of the material[21-25] or make the synthesis process more complex[16,26-27]; Doping is another common used means to enhance the cycle and rate performance of the $LiNi_{0.5}Mn_{1.5}O_4$ material, while this method also cannot avoid the disadvantages of complexification during the synthesis process,[28-32] increasing cost[33,34] and/or reducing the discharge capacity[35-37]; Appropriately magnifying particle size to decrease the contact interface with electrolyte is also constantly adopted to improve the cycle property and compaction density in practical application, nevertheless, which are usually at the cost of sacrificing capacity and rate property;[38-42] Though

nanocrystallization is applied to enhancing rate property, their high surface increases the risk of side reaction[39,43-44] and reduces Coulombic efficiency[45,46] and compaction density[15]. On the other hand, the electrode material with a yolk-shelled structure[47] can exhibit a capacity of 69.0 mAh g^{-1} even at 600 C-rate, but the volume density is too low to hinder its further application. To date, there are no reports on $LiNi_{0.5}Mn_{1.5}O_4$ materials which can resolve these contradictions in simultaneously obtaining one with high energy/power density, long lifetime and low cost. Nevertheless, it's reported that the electrochemical properties of many electrode materials are not only associated with structure, size dimension and surface property of the bulk material, but also intensely related to their crystalline orientation[45,48-49] due to the key factors of crystalline anisotropy. Recently, Lou[50] et al. reported that an anatase TiO_2 with better reversibility and excellent rate capacity can be achieved through synthesizing one holding dominant {001} surfaces. Teshima[51] and co-workers also revealed that a unique structural $LiCoO_2$ material with well developed {001}, {104}, {101}, and {102} faces can deliver a far superior rate capacity to bulk-like structure. Especially, the most inspired research is that Kanno[12,52] demonstrated a truncated octahedral structured $LiMn_2O_4$, providing a small portion of {110} surfaces whose orientations are aligned to Li diffusion channels while leaves most remaining {111} surfaces aligned along the crystalline orientations, exhibited excellent rate performance and cycle life simultaneously without other property sacrifice. However, the similar reports about $LiNi_{0.5}Mn_{1.5}O_4$ spinel are rare. Cao[53] proposed that a nanoflake-stacked $LiNi_{0.5}Mn_{1.5}O_4$ spinel with oriented growth of the {001} planes delivered greatly improved rate capacity, but these improved electrochemical properties were attributed to the very thin nanoflakes and large interspaces between the nanoflakes rather than lattice-plane anisotropy. Chen[44] investigated the rate capacities of $LiNi_{0.5}Mn_{1.5}O_4$ spinel in plate shaped with (112) surface facets and octahedral shape with (111) surface facets, but the results exhibited that the kinetic preeminence of (111) surface facets over (112). To the best of our knowledge, none of the reported $LiNi_{0.5}Mn_{1.5}O_4$ material has been researched from other surface facets, such as

{001}, {110}, {113}, {103} and so on. In the previous researches,[12,52] the {110} surface facets in $LiMn_2O_4$ spinel were regarded as one aligning to Li diffusion channels, which is beneficial to obtaining high rate capacity. Therefore, as a derivative of $LiMn_2O_4$ spinel, we speculate that the other surface facets of $LiNi_{0.5}Mn_{1.5}O_4$ spinel, such as {001}, {110}, {113}, {103} and so on, maybe also have some unknown properties in electrochemical process. To testify it, we have firstly designed a controllable approach to obtain an alternative crystal structures with micro-sized octahedral (denoted as LNMO-Oh) or pseudo-sphere liked chamfered polyhedral (denoted as LNMO-COh) $LiNi_{0.5}Mn_{1.5}O_4$ spinel through adjusting the synthetic conditions. The former exhibits a representative octahedral structure with only one type of {111} surface facets, while the latter has extra surface facets {001}, {110}, {113}, {103} and so on, and higher degree of sphericity. The electrochemical tests indicate that the micro-sized LNMO-COh possesses far superior rate capability and cycling performance to those of LNMO-Oh and these results represent the first experimental evidence for lattice-plane anisotropy in $LiNi_{0.5}Mn_{1.5}O_4$ crystal. Herein, it is worth emphasizing that the possible influencing factors to electrochemical properties except crystalline orientation can be neglected as much as possible due to the starting materials, synthesis method, crystalline structure and size dimension are the same, and the investigations of the lattice-plane anisotropy effects in $LiNi_{0.5}Mn_{1.5}O_4$ crystal have much high reliability. In addition, as we all know, the high degree of sphericity of the pseudo-sphere structure is also beneficial for obtaining high compaction density (or volumetric energy density) and excellent processability in practical application. In a word, we have firstly revealed that the micro-sized $LiNi_{0.5}Mn_{1.5}O_4$ spinel with a good compatibility between energy/power density and cycle life without any other properties sacrifice can be obtained through chamfering octahedron to pseudo-sphere liked polyhedron, and we expect that such a new approach presented here could be extended to the synthesis of various electro-active materials for usage in energy storage and conversion.

2. Experimental

2.1. Sample synthesis

The pseudo-sphere liked chamfered polyhedral $LiNi_{0.5}Mn_{1.5}O_4$ spinel (denoted as LNMO-COh) were obtained by a polymer auxiliary method. All chemicals were analytical grade and obtained from Aladdin. In a typical synthetic route, stoichiometric amounts of LiAC (0.0525 mol, excess 5% to offset the evaporation of lithium under high temperature), $Mn(AC)_2{\cdot}4H_2O$ (0.075 mol) and $Ni(AC)_2{\cdot}2H_2O$ (0.025 mol) were dissolved in distilled water (30 mL) under continuously stirring at 100 °C until a homogeneous solution was obtained. Then, $H_2C_2O_4{\cdot}2H_2O$ (0.05 mol) and PEG-400 (30 mL) were added in sequence and continuously stirring at 100 °C. Finally, a homogeneous paste was obtained after 10 h. The resulting paste was preheated at 400 °C for 1 h in air (this product was named precursor) and cooled to room temperature. After grinding 5 h by a planetary ball mill, the abovementioned precursors were further calcined under air atmosphere at 850 °C for 10 h to obtain the final products (LNMO-COh). For comparison of the influence of this unique morphology on electrochemical properties, the octahedral structure of $LiNi_{0.5}Mn_{1.5}O_4$ spinels (denoted as LNMO-Oh) were also synthesized with the same method except the process of precursor's pretreatment is under O_2 atmosphere rather than in air.

2.2. Sample characterization

X-ray powder diffraction (XRD) patterns were recorded using a Bruker D8 advance diffractometer with Cu-Kα source (λ=1.54056 Å) from 5° to 85° with a step size of 0.02° s^{-1}. Scanning electron microscope (SEM) and transmission electron microscopy (TEM) were taken on a Philip-XL30 instrument and a Tecnai G^2 F30 instrument, respectively. Raman Spectroscopy (RS) of the samples were also measured with a Raman-laser spectrometer (Renishaw inVia) using an excitation light of 633 nm from He-Ne laser. The beam power measured on the sample was around 17mW×1%. To have more reliable data, each Raman spectrum was the average of 10 scans collected at a spectral resolution of 1 cm^{-1}.

2.3. Electrochemical measurement

For the electrochemical measurement, active materials (80 wt%) were mixed and grounded with polyvinylidene fluoride (PVDF) powder (10 wt%) as a binder and acetylene back carbon (AB) powder (10wt%) as the conductive assistant materials. The mixture was spread and pressed on Al foil circular flakes as the working electrode (WE), and dried at 100 °C for 24 h under the vacuum conditions. Metallic lithium foils were used as negative electrode. The electrolyte was 1M $LiPF_6$ in a 3:7 (volume ratio) mixture of ethylene carbonate (EC) and dimethyl carbonate (DMC). The separator was UBE 3093 (Japan) micro-porous polypropylene membrane. The cells were assembled in a glove box filled with highly pure argon gas (O_2 and H_2O levels <1 ppm), and the electrochemical properties were tested in the voltage range of 4.9~3.5V (vs Li^+/Li) on a CT2001A cell test instrument (Land Electronic Co.). For the rate capability tests, the C-rates for the charge were fixed to 1C (147 mA g^{-1}) and the C-rates for the discharge were changed from 1C to 50 C. The electrochemical impedance spectroscopy (EIS) was measured with an Autolab potentiostat (PGSTAT302N, IECO CHEMIE B.V.). The impedance spectra were recorded by applying an AC voltage of 0.02 V amplitude in the frequency range of 50 mHz ~ 10^5 Hz at the end of discharge at the designated cycles. Before the XRD and SEM analyzing for the electrode after cycle test, the electrodes were disposed following: the test cells were disassembled carefully in an argon-filled grove box and thoroughly rinsed with pure DMC solvent several times to remove residual. To avoid the influence of the binder PVDF in electrodes in SEM analysis, the disassembled electrodes were washed with 1-methyl-2-pyrrolidone (NMP) by ultrasonic, centrifugal separation, repeated like that 5 times, and dried at 100 °C in an oven.

3. Results and discussion

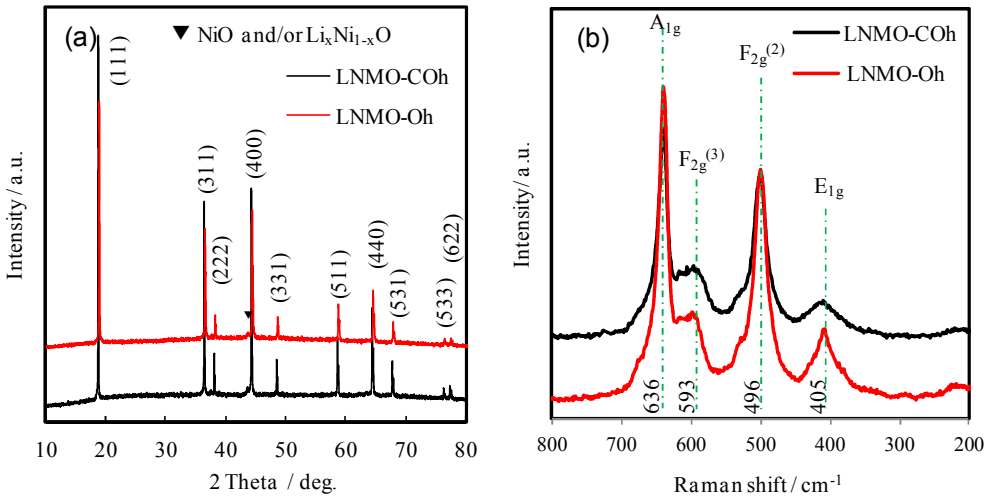

Figure 1. XRD patterns (a) and Raman spectroscopy (b) of the synthesized samples.

XRD patterns of LNMO-COh and LNMO-Oh are shown in **Figure 1**. All the samples display the typical profile of spinel phase (JCPDS card No. 80-2162). However, a small peak at 2θ=44° can not be indexed in the spinel structure but was assigned to $Li_{1-x}Ni_xO$[53,54] or NiO_x[27,55], which was a common impurity phase in LNMO products. XRD is not competent to discriminate the two phases of Fd-3m and $P4_332$ due to the scattering factors of Ni and Mn are similar,[56] while Raman and IR spectroscopy local probes sensitive to the crystal symmetry, which is a useful tool when poor chemical contrast of XRD prevents the determination of the structure (amorphous structure, cation ordering, etc.).[57] Therefore, Raman and IR (Figure S1) spectroscopy were also used to detect the phases of samples. As can be seen from Figure 1b, there were no essential difference between the two samples. According to the reports by Baudrin[56] and Julien[57], the strong band around 636 cm^{-1} was assigned to the symmetric Mn-O stretching mode of MnO_6 octahedra (A_{1g}), the big broad peak around 593 cm^{-1} was considered as $F_{2g}^{(3)}$ of the spinel compound and both peaks around 405 and 496 cm^{-1} were associated with the Ni^{2+}-O stretching mode in the structure. Based on the previous reports[56,57], the splitting of $F_{2g}^{(3)}$ band at 590 cm^{-1} was often considered as the obvious evidence of the ordered structure ($P4_332$) in the spinel, while the extra peaks at 221 and 241 cm^{-1} were also the features of $P4_332$ structure. Herein, the characteristic peaks related

to space group $P4_332$ were not detected, indicating that all the samples have a majority of Fd-3m structure (Some traced $P4_332$ may also exist, but the fraction is too small that it can be ignored). It is emphasized that the results of comparing their electrochemical properties following discussion are still reliable, because there were no essential difference in Raman and IR spectroscopy between the two samples, indicating the phase composition of both LNMO-COh and LNMO-Oh samples are the same.

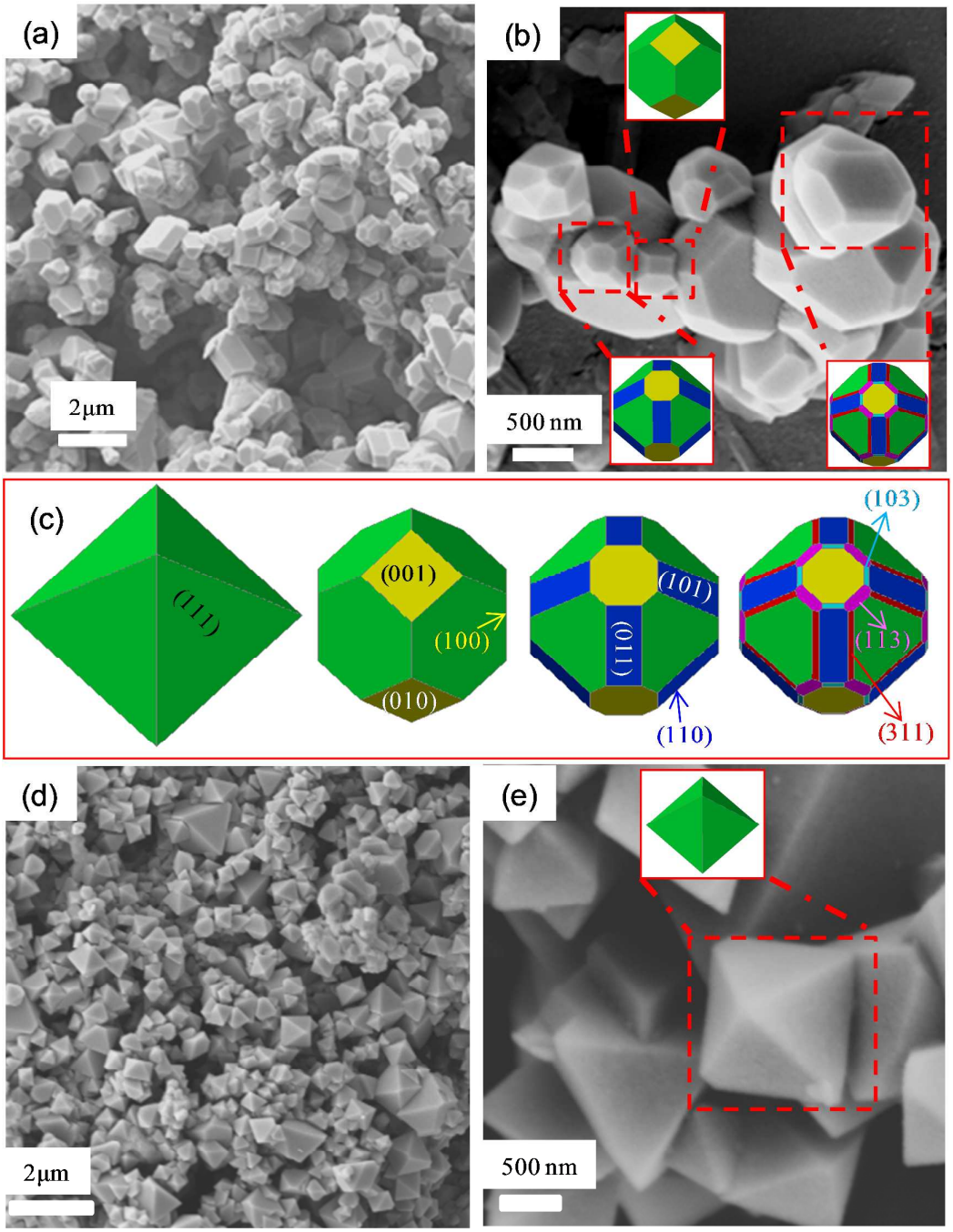

Figure 2. Low and high magnification SEM images of LNMO-COh (a and b) and LNMO-Oh (d and e); (c) the schematic drawing of LNMO with various crystal shapes.

The typical morphologies and crystal structures of LNMO-COh and LNMO-Oh were further investigated by SEM and TEM observations. As displayed in Figure 2, all samples exhibited smooth surface and uniformly distributed particles, the dimensions of LNMO-COh and LNMO-Oh were approximate ~1μm. Three types of

chamfered structure based on the parental octahedral structure can be distinctly observed from Figure 2(b), including some new crystal faces formed at the vertices and/or edges of the parental octahedral structure, also, some crystals were further chamfered at the new edges and/or vertices based on the former to form more crystal faces, resulting a pseudo-sphere particle finally. The orientation of each crystal face was assigned (Figure 2c) following the established face orientation of the octahedral face-center cubic framework, that was {111}, as well as those of its chamfered derivatives and will be further testified by TEM characterizations later. The SEM images of sample LNMO-Oh in Figure 2(d and e) revealed a representative octahedral structure, which shows only {111} crystal faces. It is worth noting that the chamfered polyhedral particles would have better fluidity and dispersivity as well as higher tap density than those of octahedral one due to the pseudo-sphere structure, indicating that the LNMO-COh has higher volumetric energy density and excellent processability than those of LNMO-Oh when applied in LIBs.

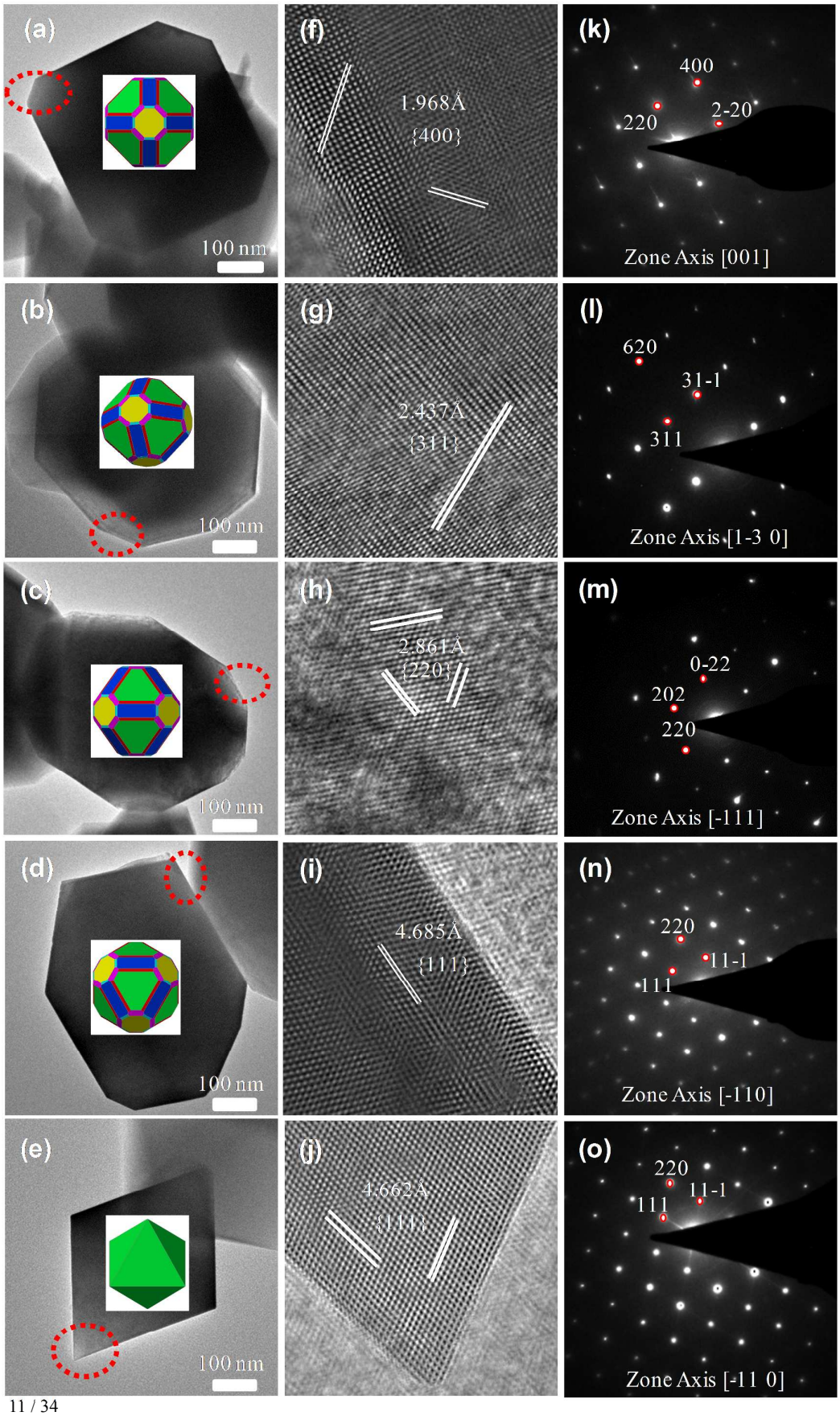

Figure 3. TEM images of LNMO-COh (a-d, f-i and k-n) and LNMO-Oh (e, j and o). (a-e) TEM images were taken at different orientations as indicated by structural schematic in each figure. (f-j) and (k-o) are HRTEM images and SAED patterns taken at red circle in a-e, respectively.

TEM observations conducted at various orientations also support the chamfered crystal structure mentioned above. Though the substantial crystal structure of most particles hindered the observation due to large dimension, some smaller particles could also be detected, as shown in Figure 3. For the sample of LNMO-COh at each orientation (Figure 3(a-d)), a high resolution TEM (HRTEM) image (Figure 3(f-i)), the resultant selected area electron diffraction (SAED) (Figure 3(k-n)), and the zone axis were attained. When viewed along the direction normal to the chamfered vertex surface (Figure 3a), a HRTEM image showed the lattice fringes with a distance of 1.968 Å along the {400} directions. The SAED pattern exhibited spots that correspond to the lattice orientations as denoted in the inset of Fig 3a. Also, the SAED pattern indicated the zone axis of the electron-beam was along the [001] direction, which was consistent with the orientation of the chamfered surface. Similarly, when viewed along the direction normal to the chamfered edge surfaces (Figure 3(b and c)) and the octahedral surface (Figure 3d), lattice fringes along the {311} (Figure 3g), {220} (Figure 3h) and {111} (Figure 3i) directions were observed, respectively. Besides, the resultant zone axis was consistent with the orientation of each chamfered surface. The same characterization was performed on the sample of LNMO-Oh (Figure 3e). As in the case of LNMO-COh (Figure 3(i and n)), HRTEM image (Figure 3j) as well as their SAED pattern (Figure 3o) and resultant zone axis of the electron-beam were obtained for LNMO-Oh, the experimental results were consistent with the properties of each crystal structure.

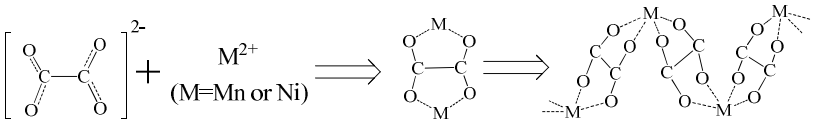

(1)

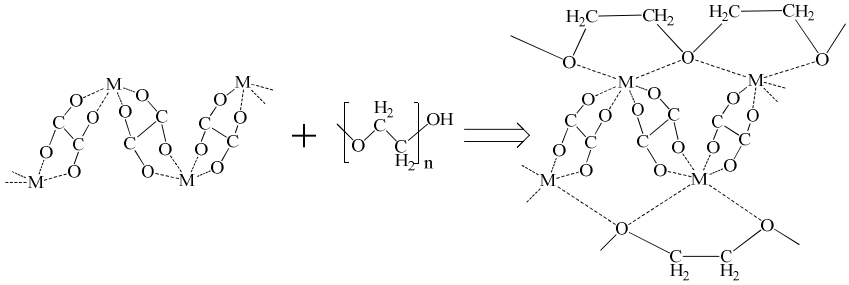

(2)

Oxalate ion is an excellent ligands for transition metal ions and has extensively applied in the synthesis of multimetallic coordination compounds,[58,59] metal-organic frameworks,[60,61] nano-materials[62,63] and so on. The acidity of oxalic acid is stronger and volatility is lower than those of acetic acid. When the oxalic acid was added into the solution containing acetic acid at 100 °C, a strong acetate smell diffuses and a lot of precipitate was formed firstly, and then the whole mixture was transformed to a homogeneous viscous liquid gradually as the reaction go on. Based on the phenomenon mentioned above, we suggest that each oxalate anion can be possibly acted as a bridging ligand to react with one metal atom to form M(ox) (M=Mn or Ni atom) precipitate firstly and then it continue to coordinate with another metal atom, finally, forming a zigzag one-dimensional chain M_2(ox) (M=Mn or Ni atom) at 100 °C heat treatment, this is also similar to the results reported by Sun et al.[58] It is worth emphasizing that the two carboxylate groups from oxalate anion could be randomly reacted with Nickel (II) ionic and Manganese (II) ionic to form an analogous heterobimetallic coordination compound due to their similar coordination ability to oxalate anion.[64,65] The reaction process would be shown as Equation (1). Attempts to identify Equation (1) directly, the Mass Spectrum (MS), Gas Chromatography (GC), Nuclear Magnetic Resonance Spectroscopy (NMR), Raman Spectroscopy (RS) should be used. However, such analyses were beyond the scope of the present paper but will be the subject of a future investigation. Nevertheless, some

indirect experiments will be discussed latter.

As an organic surfactant, PEG can act a structure-directing agent or "soft template" through adsorbing to the surfaces of growing particles or some functional groups and is widely used in preparing nanostructured materials with peculiar morphologies.[66,67] Lourdes Hernán[68] and Cao[53] have reported that PEG chains can bind to the surface of oxide nuclei through either hydrogen bonds formed by hydroxyl groups or, more probably, through interactions between oxygen-functionalized groups in the polymer and metal ions. Therefore, in the present work, the zigzag M_2(ox) chains may also be further connected with PEG to form a chain compound PEG-M_2(ox) (M=Mn and Ni atom) through interaction between oxygen-functionalized groups from the polymer and metal ions from M_2(ox) zigzag chains. A possible process of reaction and structural formula were described in Equation (2). Moreover, the lithium ions can distribute uniformly in and around this chain structure. The chain compounds with Li, Mn and Ni atoms uniformly distributed in the interiors of molecular and the carbon chain located on the surface of molecular, which were beneficial to homogeneous nucleonic reaction and unusual particle morphologies formation under high-temperature processing. Herein, it can be concluded that PEG and oxalate played important roles in the formation of the chamfered polyhedral $LiNi_{0.5}Mn_{1.5}O_4$ spinels.

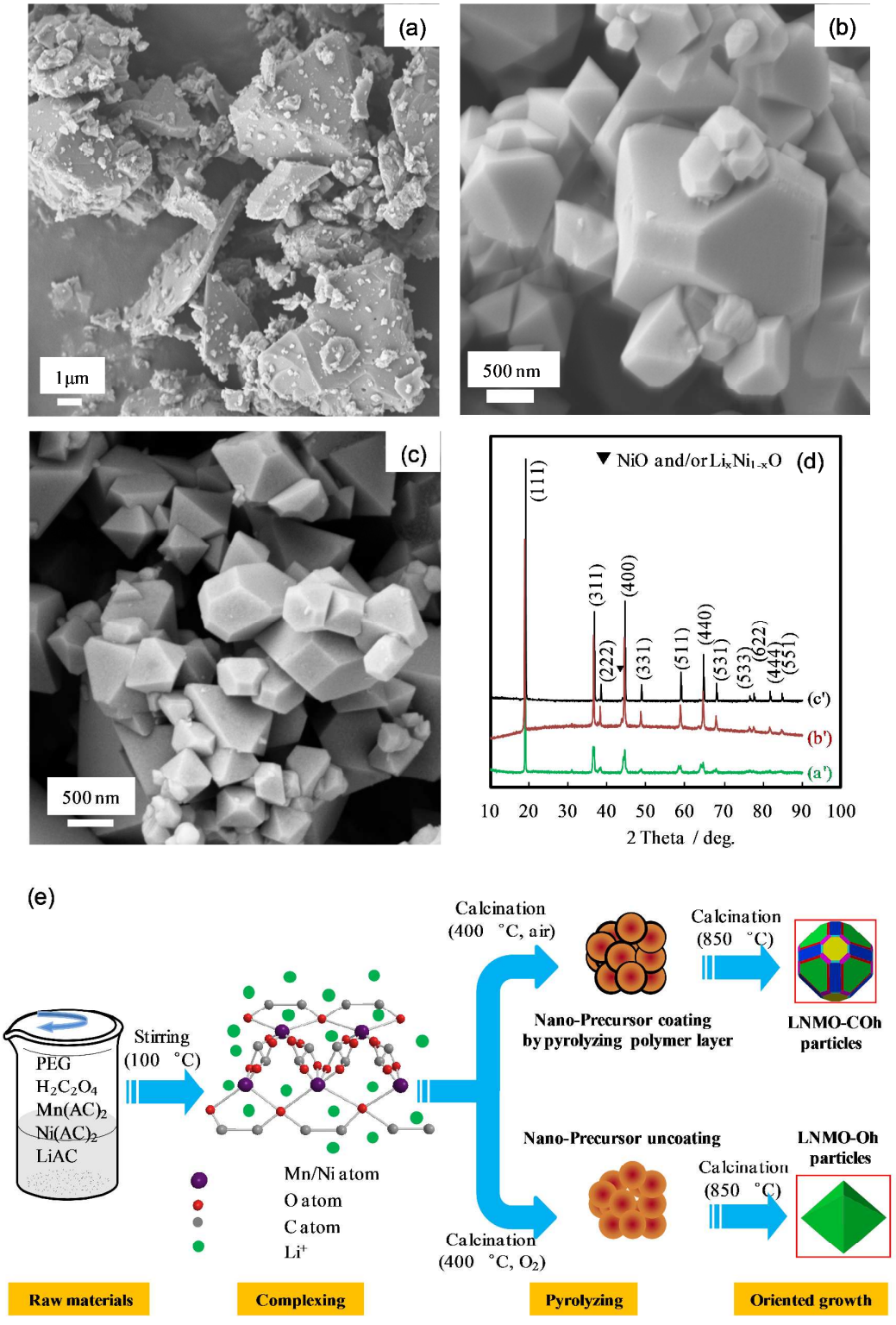

Figure 4. SEM images for the samples synthesized under different molar ratio of oxalate to metal: a) 0, b) 0.025, and c) PEG=0 mL, and their XRD patterns (d). (e) A possible model for the formation of LNMO-COh and LNMO-Oh.

To investigate the above-mentioned important roles, we designed a series of experiments. The samples with either oxalate or PEG addition were synthesized and their SEM images were shown in Figure 4(a-c), the corresponding XRD results were also shown in Figure 4d. Irregular block shaped products were obtained in the absence of oxalate addition during the synthesis process of $LiNi_{0.5}Mn_{1.5}O_4$, and some small peaks in the range of 2θ = 55-90° can not be indexed to spinel $LiNi_{0.5}Mn_{1.5}O_4$; this might be ascribed to the fact that the raw materials can not be mixed uniformly in the atomic level in absence of oxalate. When the molar ratio of oxalate to metal ions was increased to 0.025, only a half of metal ions would be reacted with oxalate anions to form zigzag $M_2(ox)$ (M=Mn and Ni atom) chains according to Equation (1), where the Li, Mn and Ni atoms were uniformly distributed in the interiors of molecular. However, the other metal ions may still distributed non-uniformly. As shown in Figure 4(b and d), the XRD pattern was in good accordance with spinel phase, spinel structured chamfered polyhedron and octahedron were coexisted and the size of particles were also uneven, which further indicate that one oxalate anion acted as a bridging ligand to link two metal atoms in forming a zigzag one-dimensional chain. It seems that forming zigzag one-dimensional chain was the most effective way to get homogeneous nucleonic reaction which was crucial for obtaining a uniform product both in morphology and dimension. Figure 4c shows the sample obtained in absence of PEG during the synthetic process, chamfered polyhedron and octahedron coexisted can be seen from the SEM images, while the particles distributed more uniformly (compared with the former sample in Fig 4b). These results imply that it's the oxalate anions, instead of the PEG, which may be only served as a structure-directing agent, played a crucial role in forming uniform products. In addition, the facts that some of octahedral spinels were also transformed to chamfered polyhedral spinels in the absence of PEG might be attributed to the residual carbonaceous organic material which came from the pyrolysis of oxalate or acetate under low temperature sintering. To further investigate the role of PEG and oxalate in the formation of chamfered $LiNi_{0.5}Mn_{1.5}O_4$ spinels, a new experiment was designed and executed,

namely, the synthetic conditions were not changed except the precursor pretreatment atmosphere. In this synthetic route, air and oxygen were used in the pretreatment process, and found that oxygen was more efficient for removing the residual carbonaceous organic from PEG, oxalate or acetate. Though the phase structures and morphologies of these precursors were similar (see in Electronic supplementary information, Figure S2), the morphologies of the obtained final products were quite different. As described above (Fig 2(d and e)), the morphology of final product obtained from precursor processed under oxygen gas was a typical regular octahedron and the size of particles was also uniform. This result suggested that the residual carbonaceous organic materials from PEG or oxalate or acetate could tailor the octahedral morphology to chamfered polyhedron. Especially, the PEG located on the surface of PEG-M_2(ox) (M=Mn and Ni atom) was more conducive for the formation of chamfered polyhedron. Other synthetic conditions such as calcination temperature were also discussed in Figure S3 (Electronic supplementary information), suggesting that the calcination temperature was not a determining factor for the formation of chamfered polyhedral morphology.

Based on the results mentioned above, a possible model for the formation of chamfered polyhedron $LiNi_{0.5}Mn_{1.5}O_4$ spinel was proposed, and can be described as a growth of Complexing-Pyrolyzing-Oriented in Figure 4e. Firstly, each oxalate anions acted as a bridging ligand to link two metal atoms at 100 °C to form zigzag M_2(ox) (M=Mn and Ni atom) chains, and then it further interacted with PEG to generate a chain compound PEG-M_2(ox) (M=Mn and Ni atom); Secondly, these compounds were transformed into nano-particles coating by pyrolyzing polymer layer under air atmosphere after a process of pyrolysis was executed at a low temperature (below 400 °C), while only nano-particles were obtained under O_2 atmosphere. Finally, the octahedral $LiNi_{0.5}Mn_{1.5}O_4$ spinels were formed from the precusor without coating under high-temperature calcinations, while the chamfered polyhedron $LiNi_{0.5}Mn_{1.5}O_4$ spinels were obtained from the percuser coating by pyrolyzing polymer layer based on the modifying growth kinetics and favoring anisotropic growth of crystals by

the pyrolyzing polymer layer.

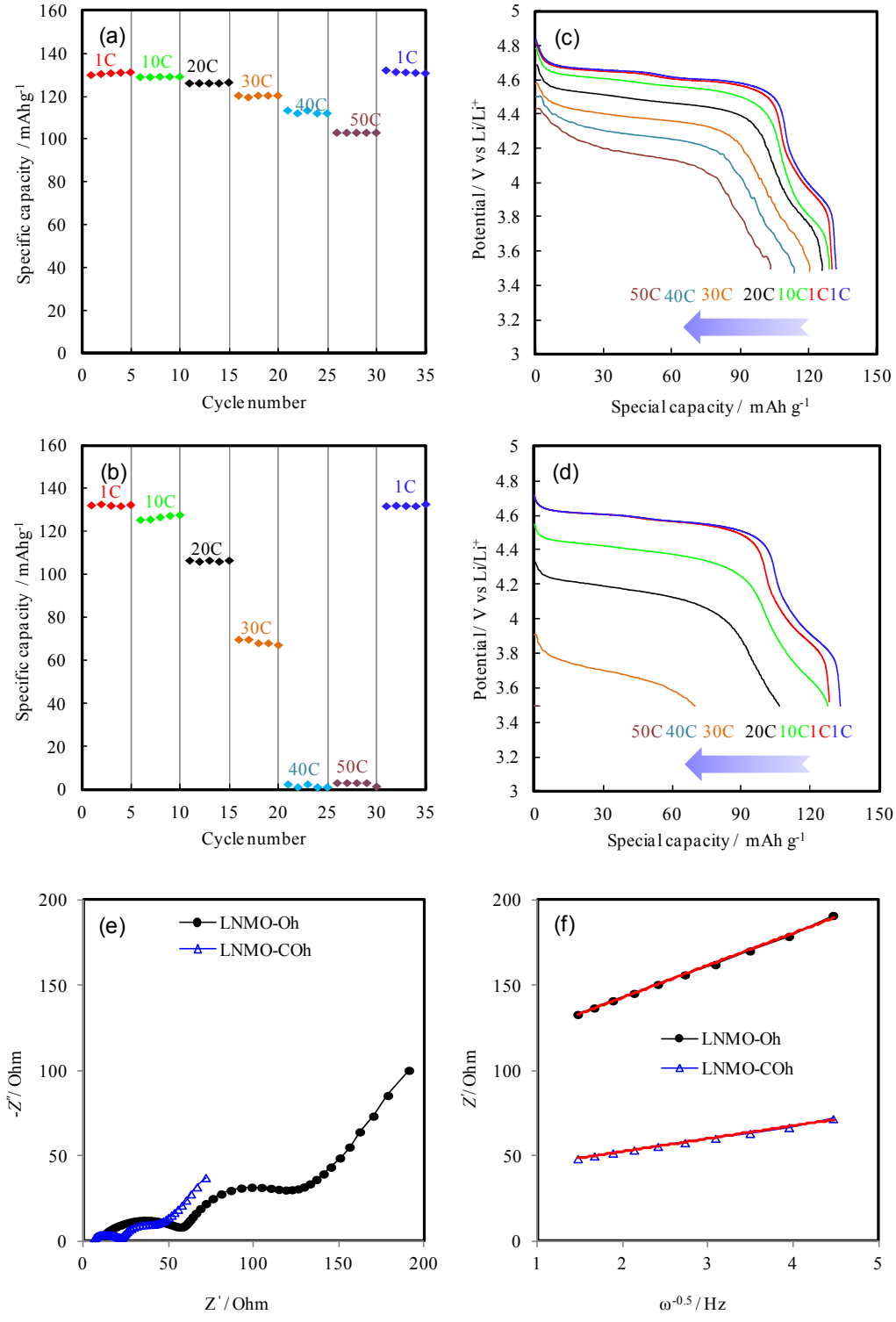

Figure 5. The rate capability of LNMO-COh (a) and LNMO-Oh (b), respectively; and their corresponding

representative discharging profiles (c) and (d); Nyquist plots for the LNMO samples after rate testing (e); Slope of the plots of Z' against $\omega^{-1/2}$ (f).

It has been found that the well-established 3D ionic channels can endow the spinel with a remarkable rate performance. Motivated by the impressive results reported previously,[52] we have also investigated the rate performance of LNMO-COh and LNMO-Oh composites under different C-rates. As shown in Figure 5a, the LNMO-COh cathode can still achieve a capacity of 103 mAh g^{-1} even the discharge current density at a very high rate of 50 C, which is equal to 79.3 % of the capacity discharged at 1 C. The capacity retention was also quite remarkable and was also better than that of the similar material with much smaller particle size reported previously.[15,46,55,69] By contrast, the discharge capacity of LNMO-Oh cathode (Figure 5b) presented only 69 mAh g^{-1} at a rate of 30 C and even less capacity at 50 C. Besides, the LNMO-COh cathode can still keep an average discharge plateau voltage of 4.1V even at 50 C, while the nearly same discharge plateau voltage appear at 20 C for the LNMO-Oh cathode (Figure 5(c and d)). The better rate capability for LNMO-COh might be mainly attributed to the unique morphology of the material. The crystal structure and grain size of both LNMO-COh and LNMO-Oh are the same, which were proved in Figure 1 to 3, indicating that their electronic conductivities in bulk material are similar. Therefore, it is easily to speculate that their different rate performance may be induced by their different lithium ion diffusion, because it was reported that the kinetics of lithium ion diffusion during electrochemical (de)intercalation was largely dependent on the lattice orientation of the surface interfacing with electrolytes.[49] In the meantime, Kanno [12] proved that the orientation of {110} surface facets in $LiMn_2O_4$ spinel were aligned to Li diffusion channels. As a derivative of $LiMn_2O_4$ spinel, thus, it's easily to assume that the {110} surface facets in $LiNi_{0.5}Mn_{1.5}O_4$ spinel are also in favor of lithium ion diffusion comparing to {111} surface facets. Moreover, for $LiNi_{0.5}Mn_{1.5}O_4$ crystal, though the detailed evaluation of the roles of the crystal surface facets in Li-ion transport has not yet been reported, we anticipated that some of the new crystal

orientations, such as {001}, {113}, {103} and so on, also were possibly beneficial to lithium ion diffusion during electrochemical (de)intercalation. To versify our speculation, the EIS measures after rate testing were carried out, as shown in Figure 5e. From the Nyquist plots, the straight line at low frequencies is attributed to the diffusion of lithium ions. The lithium ion diffusion coefficient (D_{Li}) in the $LiNi_{0.5}Mn_{1.5}O_4$ electrode could be calculated by Equation 3:

$$D_{Li} = \frac{R^2T^2}{2A^2n^4F^4C^2\sigma^2} \quad (3)$$

Where R is the gas constant, T is the room absolute temperature in our experiment, A is the surface area of the electrode, n is the number of electrons per molecule attending the electronic transfer reaction, F is Faraday constant, and C is the concentration of lithium ion in the $LiNi_{0.5}Mn_{1.5}O_4$ electrode. The σ could be calculated by Equation 4:

$$Z' = R_S + R_{ct} + \sigma\omega^{-1/2} \quad (4)$$

Table 1 σ values and the apparent diffusion coefficients of lithium ion for LNMO-COh and LNMO-Oh by EIS.

Samples	LNMO-COh	LNMO-Oh
A (cm^{-2})	1.13	1.13
C (mol/cm^{-3})	0.001	0.001
σ	18.876	7.562
D_{Li} (cm^{-2} s^{-1})	4.843E-10	7.774E-11

The σ, presented in Table 1, is the slope of the plots of Z' against $\omega^{-0.5}$, which was shown in Figure 5f. The diffusion coefficients of lithium ions calculated by Equation 3 for both LNMO-COh and LNMO-Oh were presented in Table 1. The results showed that the lithium ion diffusion coefficient (D_{Li}) of LNMO-COh (4.843×10^{-10}) is 6.3 times higher than that of LNMO-Oh (7.774×10^{-11}) and also slight higher than that of other groups[70],

indicating that the enhanced rate performance in present work can be attributed to crystalloplanar anisotropy of lithium ions diffusion. That's why the chamfered polyhedral $LiNi_{0.5}Mn_{1.5}O_4$ has a far superior rate capability to the octahedral one.

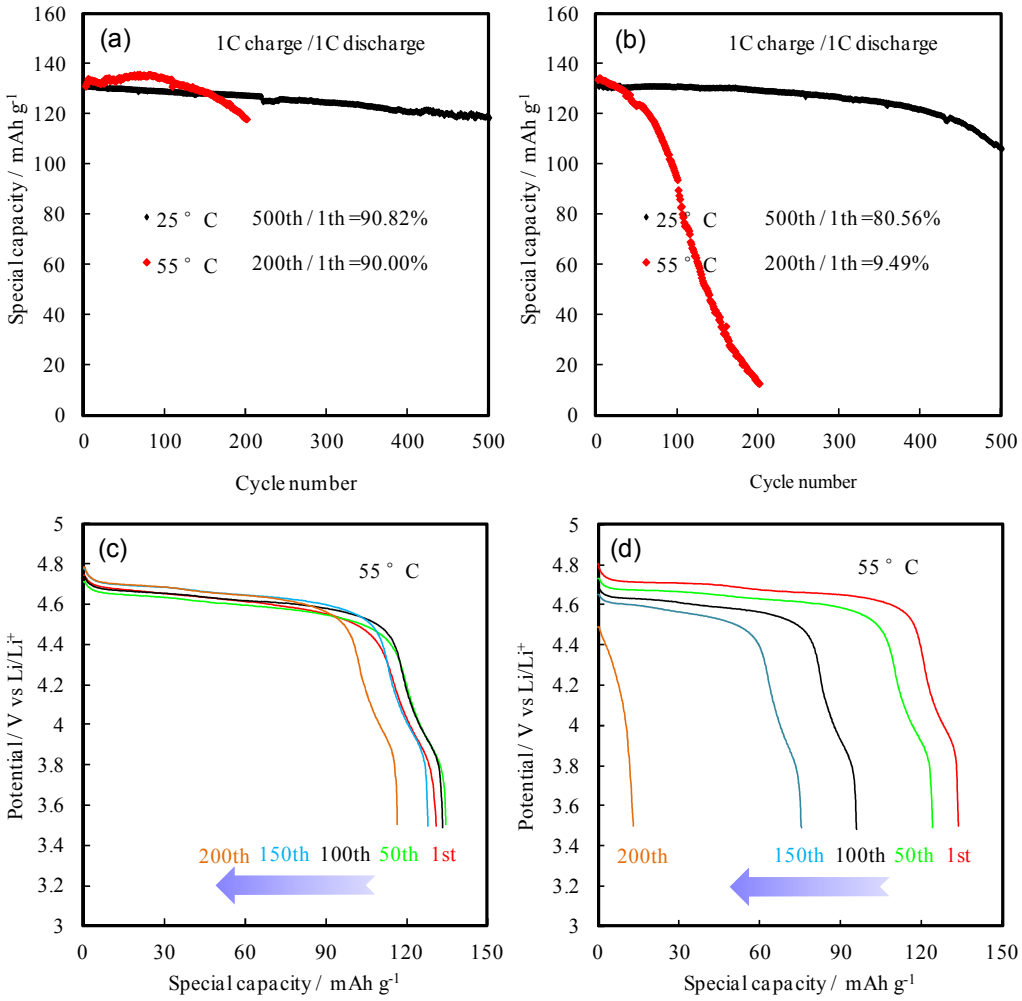

Figure 6. The cycle performances of the LNMO-COh (a) and LNMO-Oh (b) at 25 and 55 °C, respectively; the corresponding representative discharging profiles at 55 °C for LNMO-COh (c) and LNMO-Oh (d).

In order to obtain an overall evaluation of the electrochemical performance of LNMO-COh and LNMO-Oh cathodes, the cycling performances were also tested by employing 1 C current density at 25 and 55 °C, respectively. It's obviously exhibited that LNMO-COh provided more excellent cycle performances both at 25

and 55 °C than those of LNMO-Oh, as depicted in Figure 6(a and b). The capacity retentions of LNMO-COh were 90.82 % after 500 cycles when cycled at 25 °C and 90.00 % after 200 cycles under 55 °C (Figure 6a). For the sample LNMO-Oh, the capacity retention was only 80.56 % after 500 cycles when cycled at 25 °C, a slight inferior to the property of LNMO-COh. However, the discharge capacity dropped quickly as the cycle number increase when the testing temperature was increased to 55 °C (Figure 6b). The corresponding representative discharging profiles of both samples at 55 °C were presented in Figure 6(c and d), it clearly shows that, the main discharge plateau voltage, which is an important index for evaluating the polarization situation of the material, was always maintained at nearly 4.7 V before 200 cycles for LNMO-COh cathode, while the discharge plateau voltage drops quickly along with the cycle proceeding for LNMO-Oh cathode, indicating the big polarization existed in the bulk material. The increased polarization may be caused by the change of surface structure, which will be discussed in the following by EIS and SEM methods.

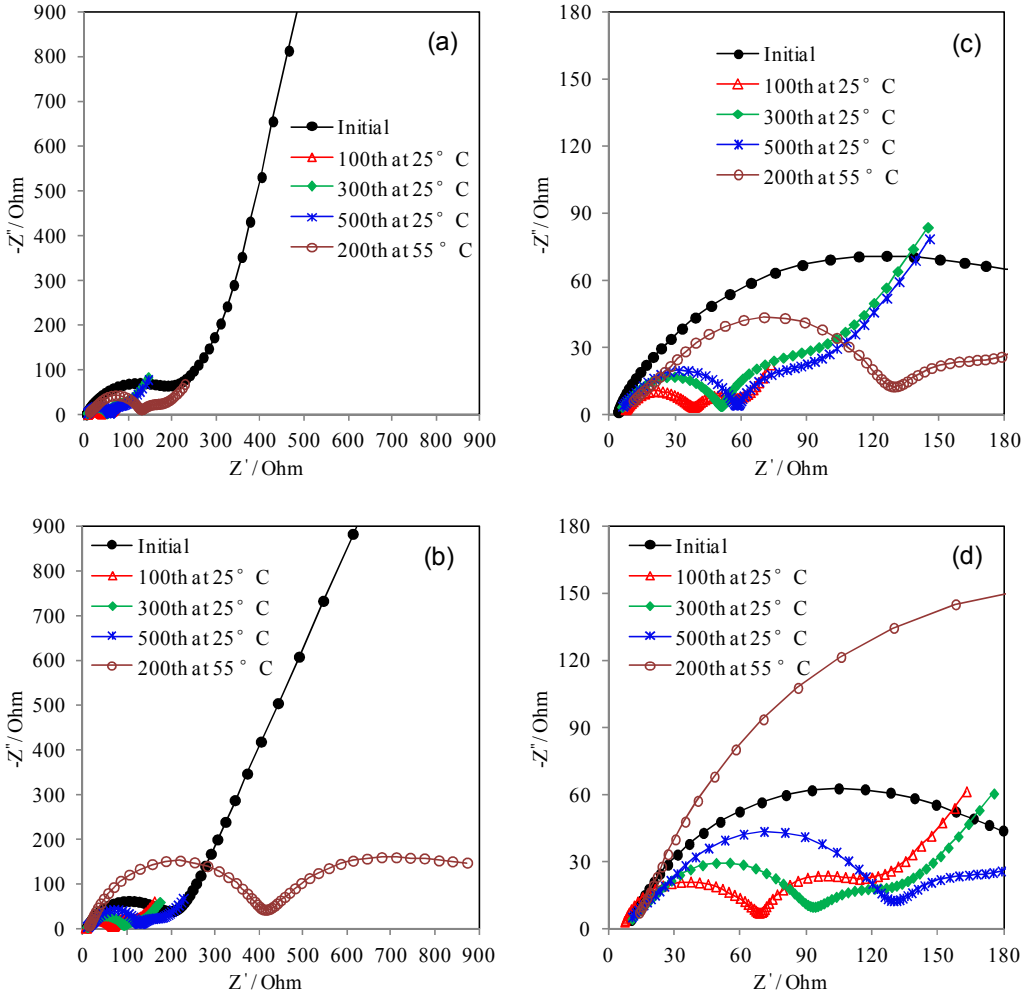

Figure 7. EIS results for $LiNi_{0.5}Mn_{1.5}O_4$ with different morphologies during cycling: (a) LNMO-COh; (b) LNMO-Oh; (c-d) magnified sections for LNMO-COh and LNMO-Oh.

To better understand the electrochemical properties of the materials, EIS measurements of both samples were conducted. The cells were cycled at 25 and 55 °C, and then fully discharged to 3.5 V prior to EIS measurements, the EIS results of the cells before electrochemical test and cycled after 100th, 300th and 500th at 25 °C and cycled after 200th at 55 °C are shown in Figure 7. As reported previously,[9,71] the first semicircle of impedance spectra at high frequency was attributed to the Li ions migration through the SEI layer (R_{SEI}), and the diameter of the second semicircle at middle-range frequency represented charge transfer resistance between the cathode active materials and liquid electrolyte (R_{ct}), the rising line in the low-frequency region was related to the solid-state

diffusion of Li ions in the electrode materials. It can be seen that, though both of samples showed the largest semicircle diameters prior to any electrochemical tests at 25 °C, the sample LNMO-Oh exhibited a persistent increase in the R_{SEI} throughout cycling (ΔR_{SEI} = R_{SEI} (500th cycle)-R_{SEI} (100th cycle) ≈ 64.2 Ohm), while the LNMO-COh exhibited a more stable behavior (ΔR_{SEI} = R_{SEI} (500th cycle)-R_{SEI} (100th cycle) ≈ 21.9 Ohm). When testing after 200 cycles at 55 °C, a similar but more severe phenomenon appeared that the ΔR_{SEI} of LNMO-Oh was equal to 335.43 Ohm, while the ΔR_{SEI} of LNMO-COh was only 91.5 Ohm comparing with those after 100 cycles at 25 °C. The sharp capacity fading for the LNMO-Oh could be related to the interfacial side reaction between the surface of active material and liquid electrolyte during cycling process, which results in the continued growth of undesired SEI layer functioning as a resistive layer for ionic conduction. In addition, the R_{SEI} of LNMO-COh at each stage was lower than those of LNMO-Oh. It seems that the chamfered polyhedral spinel with extra crystal faces, such as {110}, {001}, {113}, {103} and so on, has smaller interfacial resistances compared to that of only {111} crystal face.

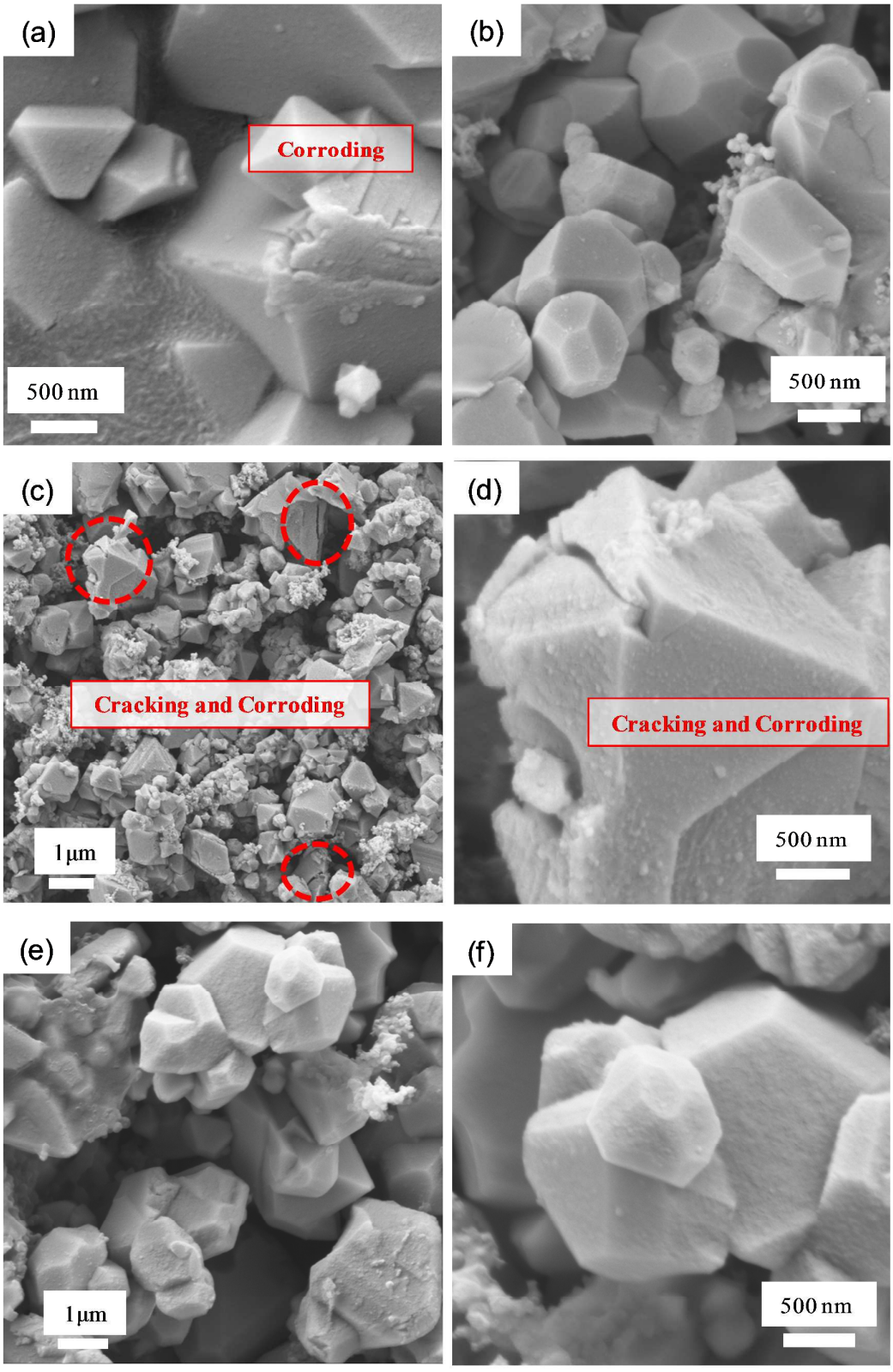

Figure 8. SEM images of the LNMO electrodes after different cycling tests: (a) LNMO-Oh and (b) LNMO-COh after 500 cycling at 25 °C, respectively; (c-d) LNMO-Oh and (e-f) LNMO-COh after 200 cycling at

55 °C, respectively.

Generally, the reasons for the capacity fading of spinel cathode are believed to be the large lattice strain during the charge-discharge process,[49,72-74] and the corrosion reaction between the cathode surface and the electrolyte during the charge-discharge process.[13] To observe structural changes during the cycling process, the cells were disassembled after designed cycles and the positive electrodes were analyzed by XRD and SEM measurements. As shown in Figure S4 (Electronic supplementary information), all the samples presented well-defined cubic spinel patterns without obvious change, indicating that the crystal structure of both of LNMO-COh and LNMO-Oh are stable. Figure 8 depicts SEM images of the LNMO-COh and LNMO-Oh after cycling test, a clear evidence of damage on the edge of the LNMO-Oh particles (Figure 8a) after 500 cycles at 25 °C was observed, while the particles of the LNMO-COh (Figure 8b) maintained their original status. Moreover, this phenomenon becomes more severe after 200 cycles at 55 °C. A serious cracking accompanied corrosion on the surface for the LNMO-Oh particles was found, as depicted in Figure 8(c and d). However, the LNMO-COh particles (In Figure 8(e and f)) still maintained their original status with smooth surface. In fact, the cracking particles could further accelerate the surface corrosion due to the development of SEI layers on the new formed surface, leading to poor contact between the active materials and the conductive agent or current collector,[75] which was also accord with the result of EIS (in Figure 7) that the cell impedance of LNMO-Oh increased more faster than that of LNMO-COh. Therefore, these results indicated that the surface corrosion and cracking were the main reason for the capacity fading of LNMO-Oh particles both at 25 and 55 °C. However, the primary cause of their difference on the stability of surface structure during charge-discharge process is still unclear, and no published results are available for the properties on each crystal face of $LiNi_{0.5}Mn_{1.5}O_4$ during cycling process. Recently, similar research[76] on $LiMn_2O_4$ spinel has been investigated by atomistic simulation method, which showed that the {111} crystal faces of the spinel possesses the highest surface energy and would

undergo the most extensive rearrangements when soaked into electrolyte. These results might lead to two consequences: i) the Mn ions on the surface of (111) are predominantly trivalent; ii) the Mn ions on the surface of (111) are coordinated in distorted square-planar complexes. The former might accelerate surface corrosion owing to the Jahn-Teller distortion by Mn^{3+}, while the latter might make the (111) crystal face suffer from severe lattice strain and tend to crack to release extra energy. It's interesting that our experimental results for $LiNi_{0.5}Mn_{1.5}O_4$ spinel are consistent well with the simulation results in $LiMn_2O_4$ spinel. Therefore, the improved cycling performance of LNMO-COh might be attributed to the facts that the reduced ratio of {111} surface facets in chamfered polyhedral structure, which can suppress the lattice strain and Mn dissolution during the charge-discharge process. In addition, the specific surface area of chamfered polyhedral particles would be also smaller than that of octahedral particles due to its pseudo-sphere structure, which is beneficial to reducing the side reaction between cathode surface and the electrolyte at high operating voltage (~5V).

4. Conclusions

In summary, we have firstly reported a controllable method to synthesize an alternative micro-sized $LiNi_{0.5}Mn_{1.5}O_4$ spinel with octahedral structure (showing only one type of {111} surfaces) or pseudo-sphere liked chamfered polyhedral structure (possessing extra surfaces {001}, {110}, {113}, {103} and so on). A possible growth model, Complexing-Pyrolyzing-Oriented, for the formation of chamfered polyhedral $LiNi_{0.5}Mn_{1.5}O_4$ spinel was proposed based on a series of the experimental results. The electrochemical properties of the chamfered polyhedral and octahedral $LiNi_{0.5}Mn_{1.5}O_4$ spinel were investigated. Results showed that the chamfered polyhedral $LiNi_{0.5}Mn_{1.5}O_4$ has a far superior rate capability to the octahedral one, attributing to the existence of new crystal orientations {110}, which would be more beneficial to lithium ion diffusion. Besides, the chamfered polyhedral $LiNi_{0.5}Mn_{1.5}O_4$ has more excellent cycling life both at 25 and 55 °C than those of octahedral one due to the reduction of {111} surface facets, which can suppress Mn dissolution and lattice strain

coming from the Jahn-Teller distortion by Mn^{3+} during the charge-discharge process. In addition, the pseudo-sphere structure is favorable for obtaining high compaction density (or volumetric energy density) and excellent processability in practical application. In particular, such a new approach presented here is also expected to use in the synthesis of various electro-active materials in energy storage filed.

Acknowledgements

This work was financially supported by the Development and Reform Commission of Guangdong Province (No.301-5), China Postdoctoral Science Foundation (No. 2013M531867), PhD Start-up Fund of Guangdong Natural Science Foundation (S2013040012451), Ministry of Education (No.20134407110006) and South China Normal University (2012KJ015 and 2013kyjj007).

The authors thank Prof. M. D. Wei for helpful discussion, who is a director of New Energy Materials Institute and the Professor in the College of Chemistry and Chemical Engineering at Fuzhou University.

Notes and references

[a] *School of Chemistry and Environment, South China Normal University, Guangzhou, 510006, PR China. Fax: 86-020-39310187; Tel:86-020-39310183; E-mail: chen829924@163.com (Zhanjun Chen); lose126@qq.com (Ruirui Zhao); dupeng.19880307@163.com (Peng Du); huhang12@gmail.com (Hang Hu); zhenren1980@163.com (Tao Wang); zhulicai@163.com (Licai Zhu); hychen@scnu.edu.cn (Hongyu Chen)*

[b] *Base of Production, Education & Research on Energy Storage and Power Battery of Guangdong Higher Education Institutes, Guangzhou, 510006, PR China. Fax: 86-020-39310187;* Tel:86-020-39310183

[c] *Engineering Research Center of Materials and Technology for Electrochemical Energy Storage of Ministry of Education, Guangzhou, 510006, PR China. Fax: 86-020-39310187;* Tel:86-020-39310183

[1] C. Liu, F. Li, L. -P. Ma and H. -M. Cheng, *Adv. Mater.,* 2010, **22**, E28.

[2] B. Dunn, H. Kamath and J.-M. Tarascon, *Science,* 2011, **334**, 928.

[3] B. Scrosati and J. Garche, *J. Power Sources,* 2010,**195**, 2419.

[4] J. B. Goodenough and Y. Kim, *Chem. Mater.,* 2010, **22**, 587.

[5] M. Park, X. C. Zhang, M. Chung, G.-B. Less and A. -M. Sastry, *J. Power Sources,* 2010, **195**, 7904.

[6] J. -M. Tarascon and M. Armand, *Nature,* 2001, **414**, 359.

[7] K. Mitzushima, P. C. Jones, P. J. Wiseman and J. B. Goodenough, *Mater. Res. Bull.,* 1980, **15**, 783.

[8] B. Kang and G. Ceder, *Nature,* 2009, **458**, 190.

[9] R. Dedryvère, D. Foix, S. Franger, S. Patoux, L. Daniel and D. Gonbeau, *J. Phys. Chem. C,* 2010, **114**, 10999.

[10] M. M. Thackeray, W. I. F. David, P. G. Bruce, J. B. Goodenough, *Mater. Res. Bull.* **1983**, *18*, 461.

[11] T. Ohzuku, J. Kato, K. Sawai and T. Hirai, *J. Electrochem. Soc.,* 1991,**138**, 2556.

[12] M. Hirayama, H. Ido, K.-S. Kim, W. Cho, K. Tamura, J. Mizuki and R. Kanno, *J. Am. Chem. Soc.,* 2010, **132**, 15268.

[13] N. P. W. Pieczonka, Z. Y. Liu, P. Lu, K. L. Olson, J. Moote, B. R. Powell and J.-H. Kim, *J. Phys. Chem. C,* 2013, **117**, 15947.

[14] J. -H. Kim, N. P. W. Pieczonka, Z. C. Li, Y. Wu, S. Harris and B. R. Powell, *Electrochim. Acta,* 2013, **90**, 556.

[15] M. G. Lazarraga, L. Pascual, H. Gadjov, D. Kovacheva, K. Petrov, J. M. Amarilla, R. M. Rojas, M. A. Martin-Luengo and J. M. Rojo, *J. Mater. Chem.,* 2004, **14**, 1640.

[16] T. Y Yang, N. Q. Zhang, Y. Lang and K. N. Sun, *Electrochim. Acta,* 2011, **56**, 4058.

[17] J. Guan and M. Liu. *Solid State Ionics,* 1998, **110**, 21.

[18] J. M. Zheng, J. Xiao, X. Q. Yu, L. Kovarik, M. Gu, F. Omenya, X. L. Chen, X. Q. Yang, J. Liu, G. L. Graff, M. S. Whittinghamc and J. -G. Zhang, *Phys. Chem. Chem. Phys.,* 2012, **14**, 13515.

[19] M. S. Whittingham, *Chem. Rev.,* 2004, **104**, 4271.

[20] G. G. Amatucci, N. Pereira, T. Zheng and J. -M. Tarascon, *J. Electrochem. Soc.,* 2001, **148**, A171.

[21] Y. -K. Sun, K. -J. Hong, J. Prakash and K. Amine, *Electrochem. Commun.,* 2002, **4**, 344.

[22] H. Sclar, O. Haik, T. Menachem, J. Grinblat, N. Leifer, A. Meitav, S. Luski and D. Aurbach, *J. Electrochem. Soc.,* 2012, **159**, A228.

[23] S. -W. Lee, K. -S. Kim, K. -L. Lee, H. -S. Moon, H. -J. Kim, B. -W. Cho, W. -L. Cho and J. -W. Park, *J. Power Sources,* 2004, **130**, 233.

[24] H. M. Wua, I. Belharouaka, A. Abouimranea, Y. -K. Sunb and K. Amine, *J. Power Sources,* 2010, **195**, 2909.

[25] J. -H. Cho, J. -H. Park, M. -H. Lee, H. -K. Song and S. -Y. Lee, *Energy Environ. Sci.,* 2012, **5**, 7124.

[26] Y. Kobayashi, H. Miyashiro, K. Takei, H. Shigemura, M. Tabuchi, H. Kageyama and T. Iwahori, *J. Electrochem. Soc.,* 2003, **150**, A1577.

[27] J. Arrebola, A. Caballero, L. Hernán, J. Morales, E. Rodríguez Castellón and J. R. Ramos Barrado, *J. Electrochem. Soc.,* 2007, **154**, A178.

[28] S. -H. Park, S. -W. Oh, S. -T. Myung and Y. -K. Sun, *Solid-State Lett.,* 2004, **7**, A451.

[29] J. Xiao, X. L. Chen, P. V. Sushko, M. L. Sushko, L. Kovarik, J. J. Feng, Z. Q. Deng, J. M. Zheng, G. L. Graff, Z. M. Nie, D. Choi, J. Liu, J. -G. Zhang and M. S. Whittingham, *Adv. Mater.,* 2012, **24**, 2109.

[30] H. L. Wang, T. A. Tan, P. Yang, M. O. Lai and L. Lu, *J. Phys. Chem. C,* 2011, **115**, 6102.

[31] O. Sha, Z. Y. Tang, S. L. Wang, W. Yuan, Z. Qiao, Q. Xu and L. Ma, *Electrochim. Acta,* 2012, **77**, 250.

[32] J. Liu and A. Manthiram, *J. Phys. Chem. C,* 2009, **113**, 15073.

[33] S. W. Oh, S. -T. Myung, H. B. Kang and Y. -K Sun, *J. Power Sources,* 2009, **189**, 752.

[34] T. -F. Yi, Y. Xie, Y. -R Zhu, R. -S Zhu and M. -F. Ye, *J. Power Sources* 2012, **211**, 59.

[35] G. B. Zhong, Y. Y. Wang, Z. C. Zhang and C. H. Chen, *Electrochim. Acta,* 2011, **56**, 6554.

[36] S. -W. Oh, S. -H. Park, J. -H. Kim, Y. C. Bae and Y. -K. Sun, *J. Power Sources,* 2006, **157**, 464.

[37] Y. Ein-Eli, J. T. Vaughey, M. M. Thackeray, S. Mukerjee, X. Q. Yang and J. McBreen, *J. Electrochem. Soc.,* 1999, **146**, 908.

[38] X. Fang, Y. Lu, N. Ding, X. Y. Feng, C. Liu and C. H. Chen, *Electrochim. Acta,* 2010, **55**, 832.

[39] Y. Talyosef, B. Markovsky, R. Lavi, G. Salitra, D. Aurbach, D. Kovacheva, M. Gorova, E. Zhecheva and R. Stoyanova, *J. Electrochem. Soc.,* 2007, **154**, A682.

[40] K. Ariyoshi, Y. Maeda, T. Kawai and T. Ohzuku. *J. Electrochem. Soc.,* 2011, **158**, A281.

[41] J. Mao, K. H. Dai and Y. C. Zhai, *Electrochim. Acta,* 2012, **63**, 381.

[42] X. H. Ma, B. Kang and G. Ceder, *J. Electrochem. Soc.,* 2010, **157**, A925.

[43] Y. G. Wang, H. Q. Li, P. He, E. Hosono and H. S. Zhou, *Nanoscale,* 2010, **2**, 1294.

[44] U. Lafont, C. Locati and E. Kelder, *Solid State Ionics,* 2006, **177**, 3023.

[45] J. Cabana, H. H. Zheng, A. K. Shukla, C. Kim, V. S. Battaglia and M. Kunduraci, *J. Electrochem. Soc.,* 2011, **158**, A997.

[46] X. K. Huang, Q. S. Zhang, J. L. Gan, H. T. Chang and Y. Yang. *J. Electrochem. Soc.,* 2011, **158**, A139.

[47] S. H. Choi, Y. J. Hong and Y. C. Kang, *Nanoscale,* 2013, **5**, 7867.

[48] L. -C. Zhang, Z. -H. Liu, H. Lv, X. H. Tang and K. Ooi, *J. Phys. Chem. C,* 2007, **111**, 8418.

[49] B. Hai, A. K. Shukla, H. Duncan and G. Y. Chen, *J. Mater. Chem. A,* 2013, **1**, 759.

[50] C. H. Sun, X. H. Yang, J. S. Chen, Z. Li, X. W. Lou, C. Li, S. C. Smith, G. Q. Lu and H. G. Yang, *Chem. Commun.,* 2010, **46**, 6129.

[51] K. Teshima, S. H. Lee, Y. Mizuno, H. Inagaki, M. Hozumi, K. Kohama, K. Yubuta, T. Shishido and S. Oishi, *Cryst. Growth Des.,* 2010, **10**, 4471.

[52] J. -S. Kim, K. S. Kim, W. Cho, W. H. Shin, R. Kanno and J. W. Choi, *Nano Lett.,* 2012, **12**, 6358.

[53] Z. X. Chen, S. Qiu, Y. L. Cao, X. P. Ai, K. Xie, X. B. Hong and H. X. Yang. *J. Mater. Chem.,* 2012, **22**, 17768.

[54] Q. Zhong, A. Bonakdarpour, M. Zhang, Y. Gao and J. R. Dahn, *J. Electrochem. Soc.,* 1997, **144**, 205.

[55] K. M. Shaju and P. G. Bruce, *Dalton Trans.,* 2008, **40**, 5471.

[56] L. P. Wang, H. Li, X. J. Huang and E. Baudrin, *Solid State Ionics,* 2011, **193**, 32.

[57] N. Amdouni, K. Zaghib, F. Gendron, A. Mauger and C. M. Julien, *Ionics,* 2006, **12**, 117.

[58] S. -S. Chen, Z. -H. Chen, J. Fan, T. -A. Okamura, Z. -S. Bai, M. -F. Lv and W. -Y. Sun, *Cryst. Growth Des.,* 2012, **12**, 2315.

[59] M. V. Marinho, T. R. G. Simões, M. A. Ribeiro, C. L. M. Pereira, F. C. Machado, C. B. Pinheiro, H. O. Stumpf, J. Cano, F. Lloret and M. Julve, *Inorg. Chem.,* 2013, **52**, 8812.

[60] J. Vallejo, I. Castro, M. Dé niz, C. Ruiz-Pé rez, F. Lloret, M. Julve, R. Ruiz-García and J. Cano, *Inorg. Chem.,* 2012, **51**, 3289.

[61] R. Otero, J. M. Gallego, A. L. Vázquez de Parga, N. Martín and R. Miranda, *Adv. Mater.,* 2011, **23**, 5148.

[62] A. Caballero, M. Cruz-Yusta, J. Morales, J. Santos-Peña and E. Rodríguez-Castellón, *Eur. J. Inorg. Chem.,* 2006, **9**, 1758.

[63] A. R. Smith, W. Yoon, W. B. Heuer, S. I. M. Baril, J. E. Boercker, J. G. Tischler, E. E. F. A. R. Smith, W. Yoon, W. B. Heuer, S. I. M. Baril, J. E. Boercker, J. G. Tischler and E. E. Foos, *J. Phys. Chem. C,* 2012, **116**, 6031.

[64] E. Coronado, J. R. Galán-Mascarós, C. J. Gómez-García and J. M. Martínez-Agudo. *Adv. Mater.,* 1999, **11**, 558.

[65] J. Martínez-Lillo, F. S. Delgado, C. Ruiz-Pérez, F. Lloret, M. Julve and J. Faus, *Inorg. Chem.,* 2007, **46**, 3523.

[66] A. Bakandritsos, A. B. Bourlinos, V. Tzitzios, N. Boukos, E. Devlin, T. Steriotis, V. Kouvelos and D. Petridis, *Adv. Funct. Mater.,* 2007, **17**, 1409.

[67] X. Gou, F. Cheng, Y. Shi, L. Zhang, S. Peng, J. Chen and P. Shen, *J. Am. Chem. Soc.,* 2006, **128**, 7222.

[68] J. C. Arrebola, A. Caballero, L. Hernán and J. Morales, *Eur. J. Inorg. Chem.,* 2008, **2008**, 3295.

[69] M. Jo, Y. -K. Lee, K. M. Kim and J. Cho, *J. Electrochem. Soc.,* 2010, **157**, A841.

[70] M. Kunduraci and G. G. Amatucci, *Electrochimica Acta,* 2008, **53**, 4173.

[71] J. Liu and A. Manthiram, *Chem. Mater.,* 2009, **21**, 1695.

[72] S. Mukerjee, X. Q. Yang, X. Sun, S. J. Lee, J. McBreen and Y. Ein-Eli, *Electrochim. Acta,* 2004, **49**, 3373.

[73] T. A. Arunkumar and A. Manthiram, *Electrochem. Solid-State Lett.,* 2005, **8**, A403.

[74] G. Amatucci and J. -M. Tarascon, *J. Electrochem. Soc.,* 2002, **149**, K31.

[75] B. Z. Li, L. D. Xing, M. Q. Xu, H. B. Lin and W. S. Li, *Electrochem. Commun.,* 2013, **34**, 48.

[76] R. Benedek and M. M. Thackeray, *Phys. Rev. B,* 2011, **83**, 195439.

The table of contents entry: (20–30 words long)

Polyhedral $LiNi_{0.5}Mn_{1.5}O_4$ exhibiting superior rate and cyclability represents the first experimental evidence for lattice-plane anisotropy.

ToC figure: